International Journal of Mass Spectrometry 296 (2010) 36–42

Contents lists available at ScienceDirect

International Journal of Mass Spectrometry

journal homepage: www.elsevier.com/locate/ijms

Gas-phase ion dynamics in a periodic-focusing DC ion guide

Joshua A. Silveira, Chaminda M. Gamage, Ryan C. Blase, David H. Russell*

Texas A&M University, Department of Chemistry, Laboratory for Biological Mass Spectrometry, College Station, TX 77843, United States

ARTICLE INFO

Article history:
Received 20 May 2010
Received in revised form 13 July 2010
Accepted 14 July 2010
Available online 29 July 2010

Keywords:
Ion mobility spectrometry
Ion guide
Periodic focusing
Effective ion temperature
Effective potential
Pseudopotential

ABSTRACT

In this work, we provide a comprehensive understanding of the radial ion focusing mechanism in the periodic-focusing DC ion guide (PDC IG). The PDC IG was developed in our laboratory to improve the sensitivity and throughput of ion mobility spectrometry (IMS) with respect to conventional uniform field IMS. Radial ion focusing, which is responsible for the sensitivity improvement, is attributed to the presence of effective potentials created by the fringing electric fields of thick ring electrodes and collisional cooling of the ions with the neutral buffer gas. The ion focusing mechanism is affirmed by investigating the variations in the effective ion temperature (T_{eff}) which are dependent upon axial position in the device. The concepts derived herein outline guidelines for the design of high performance PDC IG ion mobility instruments and other ion optical devices such as periodic-focusing DC ion funnels.

1. Introduction

Ion mobility spectrometry (IMS) is a gas-phase electrophoretic separation of ions carried out in the presence of a neutral gas, under the influence of an electric field. In the past few decades, several research groups have coupled IMS to mass spectrometry (MS) to obtain a separation dimension based on the ion-neutral collision cross-section (σ), which complements the mass-to-charge (m/z) separation of MS [1–4]. Ion mobility-mass spectrometry (IM-MS) affords several attractive analytical attributes including rapid separations of complex mixtures, isobars, and isomers, reduction of chemical noise, and determination of ion size—all of which are difficult or impossible to achieve by MS alone. Moreover, IM-MS has the capability of differentiating ions belonging to chemical classes along distinctive mobility-mass trendlines [5–7]. Although a relatively old technique, the aforementioned characteristics have allowed IMS and IM-MS to emerge as a powerful analytical tool with a broad range of applications including the study of atmospheric ions [8], aerosol particles [9], and ion cluster geometries [10–13], detection of airborne chemical agents [14,15], separation of electronic isomeric forms of small molecules [16,17], assignment of ground and excited states in transition metals [18], and characterization of hydrocarbons in crude oils [19,20]. Additionally, the separation speed and information-rich data have allowed for biological applications aimed at investigating molecular structure [21,22] and/or carrying out high-throughput separations of complex mixtures in the fields of proteomics [7,23], glycomics [24,25], and metabolomics [26].

Owing to the versatility of IM-MS, the study of novel instrument design platforms and applications continues to be one of the most rapidly growing areas in the field. Moreover, several research groups have focused on achieving high resolution ($R > 50$) IMS separations as this factor chiefly limits overall IM-MS peak capacity and the information content that can be experimentally derived [2,27,28]. The resolution of the ion mobility measurement is defined as the ratio between the average drift time, t_D, and the full width of the mobility peak at half-maximum height, Δt_{FWHM}. Theoretically, resolution is limited by several factors, although for a sufficiently small packet of ions, the dominant contribution is longitudinal diffusional broadening in the drift tube. A practical definition of resolution in terms of experimental parameters is given by [29],

$$R = \frac{t_D}{\Delta t_{FWHM}} = \left(\frac{LEq}{16 \ln 2 K_B T}\right)^{1/2} \quad (1)$$

where T is the temperature, q is the ion charge, K_B is Boltzmann's constant, L is the length of the drift tube, E is the electric field, and the product LE translates into the overall voltage drop, V, across the drift tube. Hence, Jarrold and coworkers reported among the highest measured mobility resolution to date, 172, for singly charged fullerene radical cations using 10,000 V applied across a 63 cm drift tube maintained at a pressure of 500 Torr [28] while Clemmer and coworkers recently achieved a mobility resolution of 345 for the

* Corresponding author at: Texas A&M University, Interdisciplinary Life Sciences Building, 3474 TAMU, College Station, TX 77843-3474, United States.
Tel.: +1 979 845 3345.
E-mail address: russell@chem.tamu.edu (D.H. Russell).

1387-3806/$ – see front matter © 2010 Elsevier B.V. All rights reserved.
doi:10.1016/j.ijms.2010.07.019

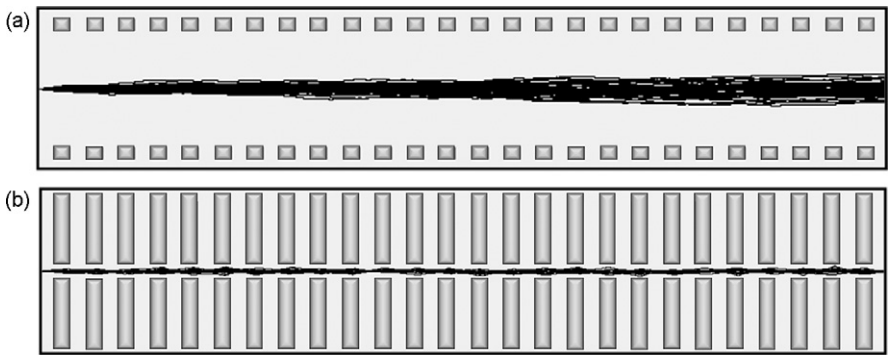

Fig. 1. Longitudinal cross-sections of uniform field (a) and periodic-focusing field (b) IMS drift tubes showing ion trajectories in black. Ion transmission is increased in the PDC IG *via* the periodic-focusing mechanism which confines ions near the central drift axis and maximizes ion transport through the exit of the drift tube.

(+2) charge state of Substance P using a pulsed cyclic drift tube design [30].

Sensitivity, however, is the most sacrificed analytical figure of merit in high resolution IM-MS, owing to the loss of radially-diffuse ions at conductance limiting apertures required for efficient integration of the relatively high pressure drift tube and the vacuum region of the mass analyzer. Typically, ion transmission is increased by coupling RF ion funnel interfaces at the front and/or back of uniform field drift tubes to increase ion introduction and collection efficiency prior to MS [31]. Conversely, the electrostatic periodic-focusing DC ion guide (PDC IG) incorporates two major modifications to the uniform field IMS ring electrode geometry to achieve radial confinement of ions during the IMS separation: (1) a decrease in the inner diameter and (2) an increase in the thickness of the lens element with respect to the electrode spacing, while a linear axial voltage drop is maintained across the electrode stack [32,33]. The novel geometry takes advantage of the fringing electric fields created near the edges of thick electrodes that generate the periodic-focusing phenomenon. As a result, the PDC IG can operate in the low pressure regime between 1 and 10 Torr to produce rapid IMS separations on the μs–ms timescale and allow for utilization of kHz electronic pulsing and/or various multiplexing strategies for ion injection into the drift tube [34,35]; under these conditions, the signal-to-noise is greatly enhanced and the duty cycle of the IM-MS instrument can approach unity.

Fig. 1 contains simulated ion trajectories in the PDC IG and uniform field IMS drift tubes. The ion trajectories illustrate that the PDC IG yields increased ion transmission compared to uniform field IMS and our most recent investigations show up to a 40-fold increase in ion transmission with only a 10% decrease in resolution [36]. The PDC IG has been used for rapid IMS separations of fullerene and model peptides with mobility resolution up to 80 for a 1.25 m length drift tube [36]. Although excellent analytical figures of merit have been demonstrated, ion dynamics in the PDC IG have not been described in detail. In the present work, we explain the role of electrode geometry, compare radial ion confinement to the focusing mechanism in a stacked-ring DC ion guide (termed "DC IG" for simplicity), and briefly discuss the subsequent effects of radial focusing on the analytical separation as compared to uniform field IMS.

1.1. Uniform field IMS

Ion mobility separation in conventional uniform field IMS (also termed drift time IMS) occurs as ions traverse a drift tube containing an inert buffer gas under the influence of a low uniform electric field. The force exerted on the ion by the electric field is opposed by the forces created by ion-neutral collisions resulting in an average velocity for the ion, termed the drift velocity, V_D. The mobility constant, K, is the proportionality constant between the drift velocity and the electric field and is related to the collision cross-section by the following relationship [37],

$$K = \frac{V_D}{E} = \left(\frac{3q}{16N}\right) \cdot \left(\frac{1}{m} + \frac{1}{M}\right)^{1/2} \cdot \left(\frac{2\pi}{K_B T_{eff}}\right)^{1/2} \cdot \left(\frac{1}{\sigma}\right) \quad (2)$$

The terms N, m, M and T_{eff} represent particle number density of the buffer gas, the mass of the ion, the mass of the buffer gas, and the effective ion temperature, respectively. Eq. (2) is derived under the assumption that interaction potentials between ions and gas particles (*i.e.*, ion-induced dipole) are negligible—a condition that may be experimentally approached using helium as the buffer gas. Additionally, Eq. (2) applies when the kinetic energy the ions gain in the electric field ($(1/2)mV_D{}^2$) is not significantly above the thermal energy (K_BT), defining a "low field limit" which can be attained for atomic ions and IMS separations near atmospheric pressure.

Although it is generally assumed that IMS is carried out under the "low field limit", ions present in a drift tube can have a different temperature than the buffer gas (T_{eff}) owing to the electric field acting upon them [38]. Ion heating becomes significant for IMS measurements of macromolecules at reduced pressures (0.1–1 Torr). Under these conditions, $T_{eff} > T$ because the field contribution to the ion kinetic energy is nonzero. That is, the translational kinetic energy gained by a macromolecule from the electric field between subsequent collisions cannot be completely quenched by a single collision with the buffer gas; however, at sufficiently low field strength, K remains independent of E/N defining an "intermediate-field region" where Eq. (2) still applies [39,40]. In this region, variations in T_{eff} can be used to indicate fluctuations in the electric field strength and the frequency of ion-neutral collisions [41]. Here, we use T_{eff} calculations in combination with effective potentials to yield a comprehensive understanding of the ion dynamics in a PDC IG under static pressure conditions.

1.2. The concept of effective potentials

In contrast to uniform field IMS, the PDC IG contains radial focusing properties analogous to the effective potentials found in a DC IG reported by Guan and Marshall [42]. The effective potential concept, however, was originally derived to explain radial confinement of gas-phase ions moving relatively slow (or at rest) with respect to fast inhomogeneous RF (time-varying waveform) electric fields [43]. The radial effective potential, $V^*(r)$, of a multipole ion guide with an applied RF voltage is described by the relationship,

$$V^*(r) = \frac{q^2 E_0{}^2(r)}{4m\Omega^2} \quad (3)$$

where $E_0(r)$ is the amplitude of the instantaneous electric field in the radial direction and Ω is the frequency of the applied RF voltage. While $V^*(r)$ is well established for a number of electrodynamic

devices including RF ion guides [44], quadrupole ion traps [45], and RF ion funnels [46], an analogous effect is achieved for an ion moving across alternating high and low electrostatic fields, as in the DC IG. In the DC IG, ions are radially focused as they traverse thin electrodes that are alternately biased at positive and negative DC potentials. The electrostatic potentials create an effective RF potential (position-varying waveform) in the inertial frame for an ion traveling with a given axial velocity, V_Z. In a position-varying waveform, ion motion tracks with the effective RF frequency, Ω_{eff}, which is dependent upon the axial velocity of the ion and the spatial periodicity of the radial electric field, $2\pi z_0$, as follows [42],

$$\Omega_{eff} = \frac{2V_z}{z_0} \tag{4}$$

Substituting Eq. (4) into Eq. (3) and using the radial electric field, $E(r)$, to represent the radial electric field amplitude yields,

$$V^*(r) = \frac{q^2E^2(r){z_0}^2}{16m{V_Z}^2} \tag{5}$$

In the present work, we derived effective potential profiles using Eq. (5) to study the radial focusing mechanism in the PDC IG.

2. Ion dynamics simulations

2.1. Drift tube geometry

The PDC IG examined in this study consists of 26 ring electrodes with a width (w), spacing (s), and inner diameter (d) of 6 mm and an overall length of 32 cm (w:s:d aspect ratio = 1:1:1). A potential drop was applied across the electrode stack to establish a net field strength of E/p 24 V cm^{-1} Torr^{-1} corresponding to 75 Td at 298 K, unless otherwise noted.

2.2. Determination of the effective potentials

Analogous to the DC IG, the effective potentials in the PDC IG are created by the radial variations in the electric field and are dependent upon the axial velocity of the ion. The radial electric fields were determined using SIMION 8.0 (SIS, Ringoes, NJ). In SIMION, electrostatic potentials (and the electric fields) are determined by solving the Laplace equation in three dimensions [47],

$$\nabla^2 V = \nabla \cdot E = \frac{\partial E_x}{\partial x} + \frac{\partial E_y}{\partial y} + \frac{\partial E_z}{\partial z} = 0 \tag{6}$$

where the electrodes serve as the boundary conditions. It should be noted that the Laplace equation does not treat space-charge effects that may contribute to electric field variations; however, space–charge effects are minimized by performing experiments where ion densities are low. To derive the effective potential profiles, SIMION was used to calculate the radial variations in the electric field and measure the average axial ion velocity at 0.25 mm intervals along the drift tube. Since q, z_0, and m are constants in Eq. (5), the quotient, $E^2(r)/{V_z}^2$, is directly proportional to $V^*(r)$. Although the axial ion velocity values represent a radial average, the standard deviation of the measurements was low (*ca.* ±0.07 mm/μs) which implies that radial variations in the axial velocity are minimal.

2.3. Ion-neutral hard sphere collisional dynamics

Ion-neutral collisional dynamics were simulated for more than 180 periodic-focusing subunits (electrode subunits × number of ions) using $C_{60}{}^{\bullet+}$ ions (720m/z, σ = 124 Å^2) [48] and helium buffer gas with the "collision_hs1.lua" user program provided with SIMION to include ion-neutral hard sphere collisions. The effective ion temperature was determined following a procedure previously demonstrated by Fernandez-Lima et al. [41].

3. Results and discussion

3.1. Derivation of effective potentials

In our original work which first introduced the PDC IG, we indicated that the device aided in the "stabilization of ions and reduction of radial diffusion by collisional cooling in a static "pseudopotential"" [32]. However, the radial focusing mechanism was not studied in further detail. In the present work, the theoretical basis for the aforementioned statement is illustrated by deriving effective potential profiles and examining the effects of electrode geometry on the electric fields and subsequent gas-phase ion dynamics.

First, the axial (z) profile of the electrostatic potential at a constant radial (r) position alternates between high and low field regions (steep and shallow slopes, since the axial electric field is the slope of the axial potential profile) as illustrated in Fig. 2(a). Although an average electric field is applied across the entire PDC IG, the local electric field oscillates above and below the central value. The low field components are located in the middle region of the electrode while the higher field components are located in the gap between adjacent electrodes. This variation is a consequence of the finite thickness of the electrodes and results in an electric field with axial periodicity shown in Fig. 2(a). Similarly, the electrostatic potential profile and electric field variations for a DC IG at a fixed r position are shown in Fig. 2(b) [42]. Although the electrostatic potentials are different in the DC IG and PDC IG, both ultimately result in oscillating axial and radial electric fields. The spatial periodicity of the radial field generates an effective RF for an ion moving with a given axial velocity that tracks with V^* (shown later in Fig. 4). Furthermore, in the DC IG, three adjacent electrodes comprise a single effective RF spatial period (wavelength) while a single electrode and approximately half the distance to the adjacent electrode on either side comprises two wavelengths in the PDC IG. Nevertheless, Ω_{eff} is remarkably similar as both devices operate in the kHz range. Moreover, the absence of a net axial electric field in the DC IG results in ion losses for ions without sufficient initial kinetic energy and for ions whose kinetic energy is quenched by thermalizing collisions. On the other hand, Fig. 2(a) illustrates that the net electric axial field in the PDC IG oscillates about a central electric field (E_c) with an amplitude (E_0) which allows for ion transport at elevated pressures and IMS separation on the basis of σ. Initial ion kinetic energy is not critical in the PDC IG—so long as it is not sufficiently high as to result in collision-induced dissociation or structural rearrangement when determining σ. Instead, ion kinetic energy in the PDC IG is governed by E/N as in conventional IMS (see Section 1.1).

Effective potentials created by the radial variations in the electric field at the electrode edges must be considered since an effective RF alone cannot suppress radial diffusion. Fig. 3(a) illustrates that the instantaneous potential varies slightly from r = 0 to r = 1 mm off-axis indicating only slight radial variations. The deviation is more easily observed at r = 2 mm where the axial potential profile shows a decreased slope at the edges of the electrode indicating increased radial variations. Thus, the radial variations in the electric field are not significant near the central drift axis, but become increasingly important as $|r| > 0$. The radial variation of the electric field is caused by the fringing fields extending from the edges of the electrodes and is essential for producing the effective potential barriers that radially confine ions.

The alternating high and low axial electric fields result in axial ion velocities that vary with z-position in the drift tube. Compared

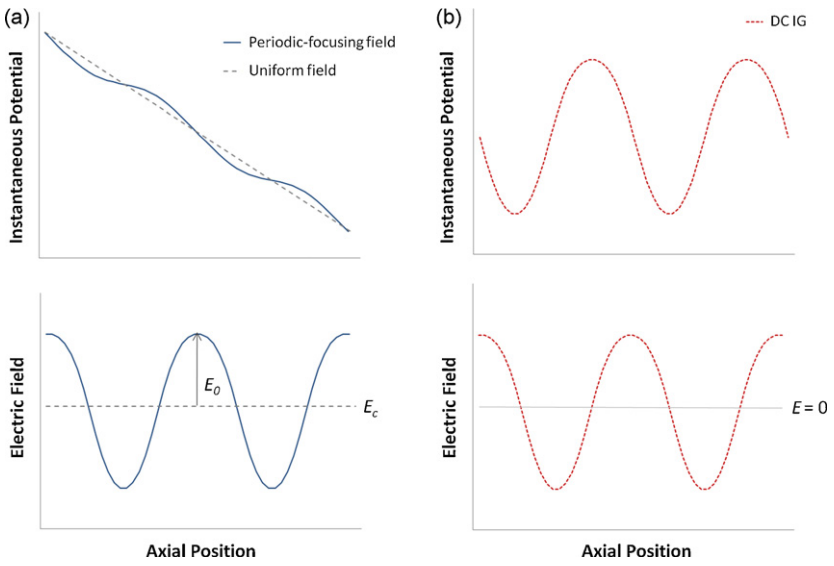

Fig. 2. Axial variations of the instantaneous voltage and the electric field shown for the PDC IG (solid blue lines) with respect to the uniform field (dashed grey lines) (a), and the DC IG (dotted red lines) (b) at fixed radial position. In both the PDC IG and DC IG, the voltage profile results in a sinusoidally oscillating electric field. (For interpretation of the references to color in the figure caption, the reader is referred to the web version of the article.)

to ions in the electrode gaps, ions inside the electrodes achieve a relatively low axial velocity in a low electric field due to a decrease in acceleration during the time period between successive ion-neutral collisions [40]. Fig. 3(b) illustrates the sinusoidal variation of the average axial ion velocity as a function of *z*-position across a single electrode subunit. It should be emphasized that the observed "deceleration" of the axial velocity is a net result of both the ion-neutral collisions and the decreasing magnitude of the electric field; therefore, for accuracy, we refer to "low axial ion velocities" rather than "deceleration" [40]. As a consequence of the low axial ion velocities, local residence time in the low electric field regions increases, exposing the ion to more collisions with the neutral buffer gas (see Section 3.2) resulting in further decreases in the ion velocity (and ion kinetic energy). Furthermore, the axial velocity of the ion at the leading edge of an electrode decreases until the ion approaches the tailing edge whereupon axial velocity increases as a result of the higher electric field that penetrates from the electrode gap. Fig. 3(b) shows that the magnitude of the axial velocity fluctuations for ions between and inside electrodes ranges from ~1.1 to 0.38 mm/μs, respectively, at E_c/N 75 Td.

The equipotential and effective potential contour profiles for a single electrode in the PDC IG are depicted in Fig. 4(a) and (b), respectively. When the axial ion velocity is considered constant, the effective potential contours appear symmetric [36]. The difference in axial velocity of the ions at the leading and tailing edge of the electrode (Fig. 3(b)) contributes to the asymmetry of the effective potentials. That is, because ions are moving with relatively lower axial velocities as they approach the tailing edge of an electrode, the magnitude of the effective potential increases, as predicted by Eq. (5). It is also important to note that the effective potentials, although asymmetric, are centered on the edges of each electrode and are negligible in the regions where the radial electric field variations are minimal *viz.* the midpoints between and inside electrodes (see Fig. 3(a)). The discontinuity in the effective potentials is a result of the thickness of the lens elements—since radial variations only occur near the electrode edges *via* fringing field effects—which has important consequences in terms of ion losses (discussed later in the text, see Fig. 5(b)). Furthermore, the effective potential profile at the edges of the electrode (without considering variations due to V_z) shows exponential decay with respect to radial position ($V^* \alpha e^r$) as expected for V^* derived for a cylindrical potential profile [42,43]. It should be noted that an exponential decay profile contains larger space–charge capacity than RF multipole devices because it more closely approaches a particle in

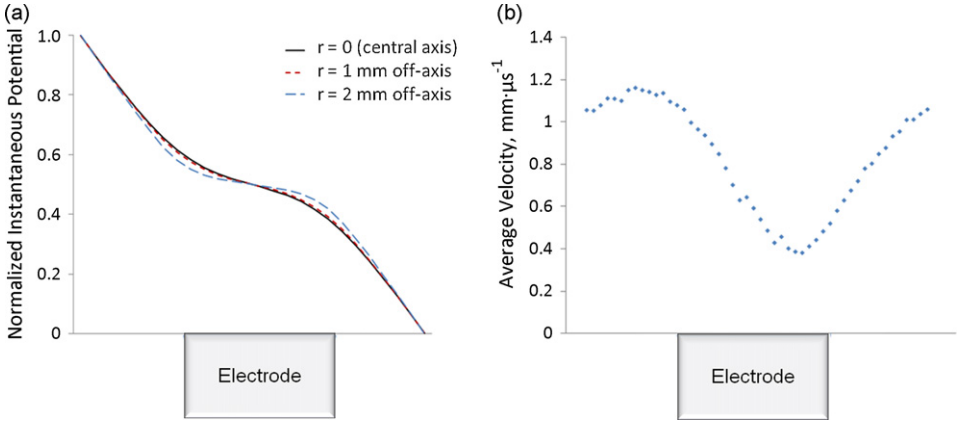

Fig. 3. Normalized axial profile of the electrostatic potential at different radial positions: $r = 0$ (solid black line), $r = 1$ (dotted red line), $r = 2$ (dashed blue line) (a), and average axial velocity of the ions (b), each shown with respect to electrode position. (For interpretation of the references to color in the figure caption, the reader is referred to the web version of the article.)

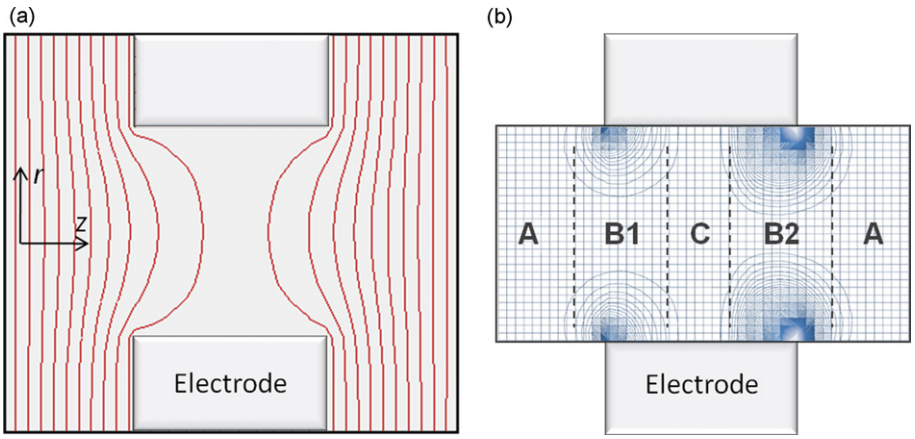

Fig. 4. "The anatomy of a periodic-focusing subunit": equipotential lines shown in red (a) and contour plot of effective potentials shown in blue (b) projected from cylindrical coordinates onto the plane of the paper and plotted with respect to electrode position. The regions which are separated by dashed lines and labeled A–C are described in Section 3.2. (For interpretation of the references to color in the figure caption, the reader is referred to the web version of the article.)

a box. That is, the radial field variations are minimal for ions on-axis while ions that deviate off-axis ($r > 0$) are confined by a steep barrier. Because the radial V^* profile deviates from a cylindrical profile away from the electrode edges, the radial electric fields are more easily obtained using SIMION calculations as opposed to modification of analytical expressions derived for an ideal cylindrical potential profile.

3.2. Periodic-focusing mechanism

Ion transport dynamics near and within each of the PDC IG electrodes appear similar, as indicated by our simulations in Fig. 1. Therefore, each electrode may be considered a single periodic-focusing subunit. To qualitatively describe the ion dynamics in the PDC IG, an electrode subunit of the drift region has been divided into four sections labeled A, B1, C, and B2, as shown in Fig. 5. In region A, the axial electric field is relatively high owing to the electrostatic potential drop from one electrode to the next. In this region, ion separation occurs on the basis of a positionally-dependent electric field where the amplitude of the axial profile of the electric field exceeds the central field ($E_{max} = E_c + E_0$). Although the ion swarm is subject to diffusional broadening in the radial and axial directions, the length of region A is relatively short and radial diffusion is corrected by the effective potentials in the subsequent regions. As ions enter an electrode (region B1) their velocity decreases as a result of the dampened electric field and ion-neutral collisions. In region C, the axial electric field amplitude defines an electric field lower than the central electric field ($E_{min} = E_c - E_0$) where ion velocities continue to decrease. The apparent radial defocusing of the ions in region C (Fig. 5(a)) is due to diffusion of the ions under these lower field conditions. It is also important to note that region C does not contain effective potentials. Thus, if the electrode thickness is increased significantly, or if E/N is decreased beyond a lower limit, region C approaches field-free conditions where diffusion will dominate. For example, in the simulation shown in Fig. 5(b), the overall average E_c/N is decreased from 75 to 37 Td to achieve low local field conditions in region C ($E_{min}/N \sim 12$ Td), while still maintaining sufficiently high field strengths for mobility separation in region A ($E_{max}/N \sim 62$ Td). In this case, thermalization may dominate for ions in region C owing to very low local electric fields and increased collisional cooling. Under these conditions some radially-diffuse ions may not have sufficient axial kinetic energy to traverse region C and/or overcome the effective potential barrier extending from the tailing edge of the electrode. These ions may follow the effective potential barriers towards the electrode surface where they are neutralized, as illustrated by the ion denoted † in Fig. 5(b). Due to the presence of low local field conditions inside electrodes, E_{min}/N is a critical parameter that affects radial focusing and ion transmission; however so long as the applied E_c/N is sufficiently large ($\gtrsim$47 Td), the ion trajectory simulations for the PDC IG investigated in this study suggest that nearly all ions ($m/z = 720$) are transmitted across the device.

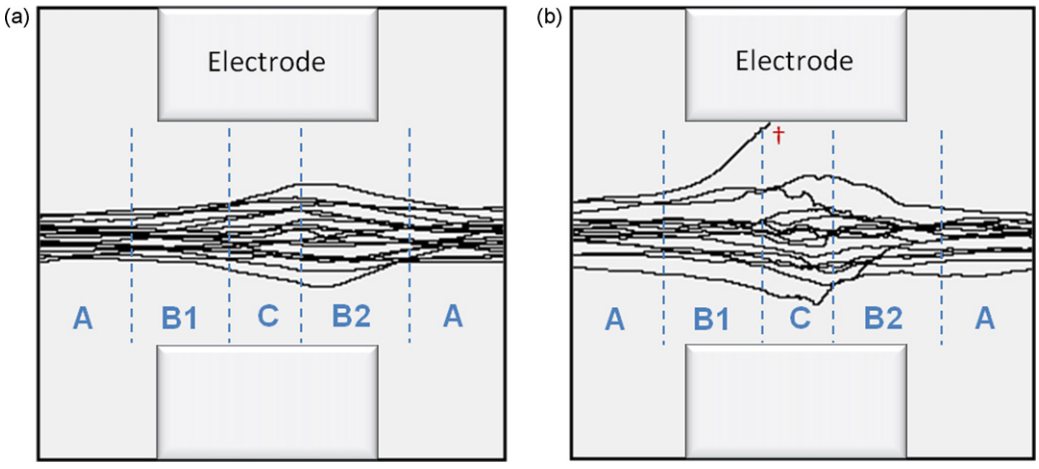

Fig. 5. Ion trajectories showing periodic-focusing subunits at varied field strength: E_c/N 75 Td (a) and 37 Td (b). In (b), the radially-diffuse ion labeled † is thermalized owing to the locally dampened electric field in region C.

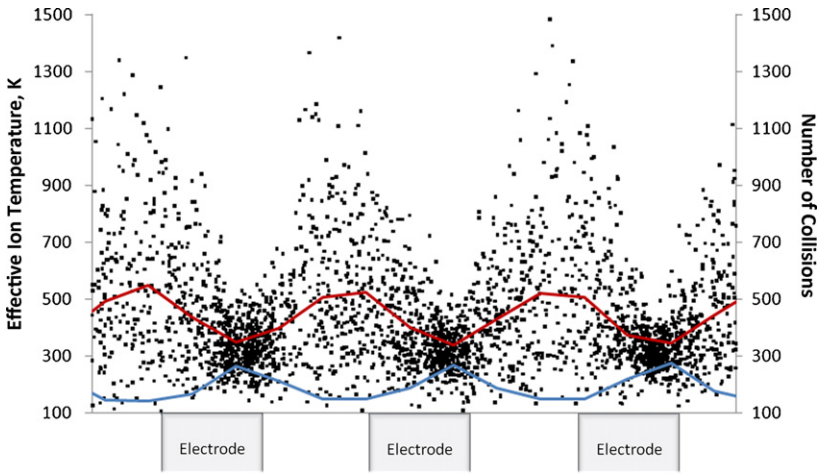

Fig. 6. Effective ion temperature of a single ion (represented with black dots) and the average of several ion trajectories (shown in red, top trace). The number of ion-neutral collisions in 0.25 mm bins is shown in blue (bottom trace) across three representative electrodes. (For interpretation of the references to color in the figure caption, the reader is referred to the web version of the article.)

3.3. Effective ion temperature and collisional dynamics

The ion dynamics described in Sections 3.1 and 3.2 are reinforced by studying T_{eff} in the PDC IG. Fig. 6 illustrates T_{eff} and the number of ion-neutral collisions with respect to the axial position for three representative electrode subunits. The observed variation in T_{eff} is a result of changes in ion velocity (or kinetic energy) initiated by the periodicity of the electric fields (Fig. 2(a)) and enhanced by subsequent collisional cooling at low axial velocities. T_{eff} reaches a minimum in region B2 and a maximum in region A, and demonstrates the periodic ion heating and cooling phenomenon inherent in the device. Fig. 6 also illustrates the inverse relationship between T_{eff} and the ion-neutral collision frequency. Although our simulations suggest that local effective ion temperatures can be high, the average T_{eff} in the PDC IG oscillates above and below ~421 K at E_c/N 75 Td. It should also be noted that for reference purposes, we also investigated the effective ion temperature in a 32 cm uniform field IMS drift tube at the same field strength, which yielded a similar average $T_{eff} \sim 438$ K. T_{eff} is expectedly greater than T (298 K) because in this field, the translational kinetic energy of $C_{60}^{\bullet+}$ cannot be entirely quenched by a single collision with a helium atom (see Section 1.1). Moreover, as expected from uniform field IMS in the "intermediate field", as E/N decreases, T_{eff} decreases proportionally, owing to a decrease in acceleration between subsequent collisions, ultimately leveling off as T_{eff} approaches T (data not shown).

3.4. IMS resolution

A comprehensive discussion of resolution and ion transmission in the PDC IG is provided by Blase et al. [36], nevertheless, several key points are evident from the ion dynamics described in this work. (1) Although the periodic-focusing field is comprised of an oscillating axial electric field (position-varying waveform), ion mobility separation occurs in all regions for the simulated geometries and local E/N values. Relatively high field IMS separation occurs in region A while regions B and C generate a combination of relatively lower field IMS separation and collisional cooling. These overall conditions produce an average drift velocity integrated over all periodic-focusing subunits and provide an efficient mobility separation with high resolution, sensitivity and throughput. (2) Based on the ion dynamics described herein, the PDC IG produces slightly lower resolution relative to uniform field IMS, owing to the radial variations in the axial electric field where the effective potentials exist leading to an increase in Δt_{FWHM} at the detector. (3) Along with the terms in Eq. (1), mobility resolution in the PDC IG is affected by the electrode inner diameter which positions the effective potentials in the radial dimension. For example, ions traversing a PDC IG with a smaller inner diameter will be more confined to the central drift axis ($r = 0$) which increases ion transmission but decreases mobility resolution. On the other hand, the converse is true for ions traversing a PDC IG with a larger electrode inner diameter.

4. Conclusions

Ion dynamics in the PDC IG are described in terms of the axial electric field variations, effective RF, discontinuous effective potentials created at the edges of the thick periodic-focusing electrodes, and the ion-neutral collisional dynamics under static pressure conditions. Our results show that the PDC IG functions analogously to a DC IG in terms of radial ion confinement, but the overall potential drop allows for ion transport at elevated pressures and creates a net electric field for IMS separation on the basis of collision cross-section. The focusing mechanism is confirmed by examining the effective ion temperature and velocity fluctuations which coincide with the effective potentials. Moreover, the PDC IG can correct the trajectory of radially-diffuse ions in one periodic-focusing subunit (a single electrode) to transport nearly all ions across the device, while a DC IG requires several effective RF cycles to obtain efficient radial focusing. Previous experimental and simulation data indicated only a small (~10% at 1 Torr) decrease in terms of resolution with respect to the uniform field IMS [36]. Our ongoing work is focused on deriving the comprehensive theory and function of the PDC IG to quantitatively explain IMS separation in the device [49].

The concepts derived to explain periodic-focusing ion dynamics herein provide insight into factors related to resolution, sensitivity, and throughput of the ion mobility separation in a PDC IG and can ultimately be used to guide future instrument development. Because of the ability to transmit nearly all ions across the entire drift length without radial broadening, we are currently investigating an increased length PDC IG (>2 m) in order to achieve higher resolution IMS separations as predicted by Eq. (1), whereas conventional uniform field drift cells of the same length may not produce an appreciable ion signal without a radial focusing mechanism. Based on the principles derived in this work, we are also currently investigating a periodic-focusing DC-only ion funnel for gas-phase ion transport across differential pressure interfaces [50].

Acknowledgement

Financial support for this work was provided by the National Science Foundation (DBI-0821700).

References

[1] P.R. Kemper, M.T. Bowers, A hybrid double-focusing mass spectrometer-high-pressure drift reaction cell to study thermal energy reactions of mass-selected ions, J. Am. Soc. Mass Spectrom. 1 (1990) 197–207.
[2] C. Wu, W.F. Siems, G.R. Asbury, H.H. Hill Jr., Electrospray ionization high-resolution ion mobility spectrometry–mass spectrometry, Anal. Chem. 70 (1998) 4929–4938.
[3] Y. Liu, D.E. Clemmer, Characterizing oligosaccharides using injected-ion mobility/mass spectrometry, Anal. Chem. 69 (1997) 2504–2509.
[4] M.F. Jarrold, V.A. Constant, Silicon cluster ions: evidence for a structural transition, Phys. Rev. Lett. 67 (1991) 2994–2997.
[5] B.T. Ruotolo, K.J. Gillig, A.S. Woods, T.F. Egan, M. Ugarov, J.A. Schultz, D.H. Russell, Analysis of phosphorylated peptides by ion mobility-mass spectrometry, Anal. Chem. 76 (2004) 6727–6733.
[6] A.S. Woods, M. Ugarov, T. Egan, J. Koomen, K.J. Gillig, K. Fuhrer, M. Gonin, J.A. Schultz, Lipid/peptide/nucleotide separation with MALDI-ion mobility-TOF MS, Anal. Chem. 76 (2004) 2187–2195.
[7] J.A. McLean, B.T. Ruotolo, K.J. Gillig, D.H. Russell, Ion mobility-mass spectrometry: a new paradigm for proteomics, Int. J. Mass Spectrom. 240 (2005) 301–315.
[8] R.C. Flagan, History of electrical aerosol measurements, Aeorosol Sci. Technol. 28 (1998) 301–380.
[9] E.O. Knutson, K.T. Whitby, Aerosol classification by electric mobility: apparatus, theory and applications, J. Aerosol. Sci. 6 (1975) 443–451.
[10] G. von Helden, M.-T. Hsu, P.R. Kemper, M.T. Bowers, Structure of carbon cluster ions from 3 to 60 atoms: linears to rings to fullerenes, J. Chem. Phys. 95 (1991) 3835–3837.
[11] A.A. Shvartsburg, M.F. Jarrold, Transition from covalent to metallic behavious in group-14 clusters, Chem. Phys. Lett. 317 (2000) 615–618.
[12] G. von Helden, P.R. Kemper, N.G. Gotts, M.T. Bowers, Isomers of small carbon cluster anions: linear chains with up to 20 atoms, Science 259 (1993) 1300–1302.
[13] F.A. Fernandez-Lima, C. Becker, K. Gillig, W.K. Russell, M.A.C. Nascimento, D.H. Russell, Experimental and theoretical studies of (CsI)(n)Cs+ cluster ions produced by 355 nm laser desorption ionization, J. Phys. Chem. A 112 (2008) 11061–11066.
[14] G.A. Eiceman, J.A. Stone, New uses of previously unheralded analytical instruments, Anal. Chem. (2004) 390A–397A.
[15] K. Cottingham, Ion mobility spectrometry rediscovered, Anal. Chem. 75 (2003) 435A–439A.
[16] J.C. May, D.H. Russell, A mass selective variable temperature drift tube ion mobility-mass spectrometer for temperature dependant ion mobility studies, Manuscript in preparation.
[17] G.F. Verbeck, K.J. Gillig, D.H. Russell, Variable-temperature ion mobility time-of-flight mass spectrometry studies of electronic isomers of Kr^{2+} and CH_3OH^{*+} radical cations, Eur. J. Mass Spectrom. 9 (2003) 579–587.
[18] J.C. May, Development of a cryogenic drift cell spectrometer and methods for improving the analytical figures of merit for ion mobility-mass spectrometry analysis, Thesis, Texas A&M University, College Station, 2009.
[19] C. Becker, F.A. Fernandez-Lima, D.H. Russell, Ion mobility-mass spectrometry: a tool for characterizing the petroleome, Spectroscopy 24 (2009) 38–42.
[20] F.A. Fernandez-Lima, C. Becker, A.M. McKenna, R.P. Rodgers, A.G. Marshall, D.H. Russell, Petroleum crude oil characterization by IMS-MS and FTICR MS, Anal. Chem. 81 (2009) 9941–9947.
[21] F.A. Fernandez-Lima, R.C. Blase, D.H. Russell, A study of ion-neutral collision cross-section values for low charge states of peptides, proteins, and peptide/protein complexes, Int. J. Mass Spectrom., 2009, in press, doi:10.1016/j.ijms.2009.10.009.
[22] L. Tao, D.B. Dahl, L.M. Pérez, D.H. Russell, The contributions of molecular framework to IMS collision cross-sections of gas-phase peptide ions, J. Am. Soc. Mass Spectrom. 20 (2009) 1593–1602.
[23] S.J. Valentine, M.D. Plasencia, X. Liu, M. Krishnan, S. Naylor, H.R. Udseth, R.D. Smith, D.E. Clemmer, Toward plasma proteome profiling with ion mobility-mass spectrometry, J. Proteome Res. 5 (2006) 2977–2984.
[24] C.S. Hoaglund, S.J. Valentine, D.E. Clemmer, An ion trap interface for ESI-ion mobility experiments, Anal. Chem. 69 (1997) 4156–4161.
[25] J. Zaia, Mass spectrometry and the emerging field of glycomics, Chem. Biol. 15 (2008) 881–892.
[26] P. Dwivedi, P. Wu, S.J. Klopsch, G.F. Puzon, L. Xun, H.H. Hill, Jr., Metabolic profiling by ion mobility mass spectrometry (IMMS), Metabolics, 4 (2008) 63–80. doi:10.1007/s11306-007-0093-z.
[27] P.R. Kemper, N.F. Dupuis, M.T. Bowers, A new, higher resolution, ion mobility mass spectrometer, Int. J. Mass Spectrom. 287 (2009) 46–57.
[28] P. Dugourd, R.R. Hudgins, D.E. Clemmer, M.F. Jarrold, High-resolution ion mobility measurements, Rev. Sci. Instrum. 68 (1997) 1122–1129.
[29] S. Rokushika, H. Hatano, M.A. Baim, H.H. Hill, Resolution measurement for ion mobility spectrometry, Anal. Chem. 57 (1985) 1902–1907.
[30] S.I. Merenbloom, R.S. Glaskin, Z.B. Henson, D.E. Clemmer, High-resolution ion cyclotron mobility spectrometry, Anal. Chem. 81 (2009) 1482–1487.
[31] S.L. Koeniger, S.I. Merenbloom, S.J. Valentine, M.F. Jarrold, H.R. Udseth, R.D. Smith, D.E. Clemmer, An IMS–IMS analogue of MS–MS, Anal. Chem. 78 (2006) 4161–4174.
[32] K.J. Gillig, B.T. Ruotolo, E.G. Stone, D.H. Russell, An electrostatic focusing ion guide for ion mobility-mass spectrometry, Int. J. Mass Spectrom. 239 (2004) 43–49.
[33] K.J. Gillig, D.H. Russell, Periodic field focusing ion mobility spectrometer, US Patent 6,639,213 (2003).
[34] J.A. McLean, D.H. Russell, Multiplex data acquisition based on analyte dispersion in two dimensions: more signal more of the time, Int. J. Ion Mobility Spectrom. 8 (2005) 66–71.
[35] J.A. McLean, D.H. Russell, T.F. Egan, M.V. Ugarov, J.A. Schultz, Multiplex data acquisition modes for ion mobility-mass spectrometry, US Patent 7,745,780 (2009).
[36] R.C. Blase, J.A. Silveira, K.J. Gillig, C.M. Gamage, D.H. Russell, Int. J. Mass Spectrom., submitted for publication.
[37] H.E. Revercomb, E.A. Mason, Theory of Plasma Chromatrography/Gaseous Electrophoresis—A Review, Anal. Chem. 47 (1975) 970–983.
[38] E.A. Mason, E.W. McDaniel, Transport Properties of Ions in Gases, John Wiley & Sons, Inc., 1988.
[39] B.T. Ruotolo, J.A. McLean, K.J. Gillig, D.H. Russell, The influence and utility of varying field strength for the separation of tryptic peptides by ion mobility-mass spectrometry, J. Am. Soc. Mass Spectrom. 16 (2005) 158–165.
[40] A.A. Shvartsburg, Differential ion mobility spectrometry, in: Nonlinear Ion Transport and Fundamentals of FAIMS, CRC Press, 2009.
[41] F.A. Fernandez-Lima, C. Becker, K.J. Gillig, W.K. Russell, S.E. Tichy, D.H. Russell, Ion mobility-mass spectrometer interface for collisional activation of mobility separated ions, Anal. Chem. 81 (2009) 618–624.
[42] S. Guan, A.G. Marshall, Stacked-ring electrostatic ion guide, J. Am. Soc. Mass Spectrom. 7 (1996) 101–106.
[43] D. Gerlich, Inhomogeneous RF Fields: A Versatile Tool for the Study of Processes with Slow Ions, State-Selected and State-to-State Ion-Molecule Reaction Dynamics. Part 1: Experiment; Advances in Chemical Physics Series LXXXII, John Wiley & Sons, Inc., 1992, pp. 1–176.
[44] Y. Huang, S. Guan, S.H. Kim, A.G. Marshall, Ion transport through a strong magnetic field gradient by r.f.-only octupole ion guides, Int. J. Mass Spectrom. Ion Processes 152 (1996) 121–133.
[45] R.E. March, J.F.J. Todd, Quadrupole Ion Trap Mass Spectrometry, second edition, John Wiley & Sons Inc., 2005.
[46] A.V. Tolmachev, T. Kim, H.R. Udseth, R.D. Smith, T.H. Bailey, J.H. Futrell, Simulation-based optimization of the electrodynamic ion funnel for high sensitivity electrospray ionization mass spectrometry, Int. J. Mass Spectrom. 203 (2000) 31–47.
[47] *SIMION*, version 8.0; Scientific Instrument Services, Inc.: Ringoes, NJ, 2006.
[48] L. Tao, J.R. McLean, J.A. McLean, D.H. Russell, A collision cross-section database of singly-charged peptide ions, J. Am. Soc. Mass Spectrom. 18 (2007) 1232–1238.
[49] C.M. Gamage, R.C. Blase, J.A. Silveira, D.H. Russell, Thermodynamic Properties of Ions in a Periodic-Focusing DC Ion Guide, Manusctipt in preparation.
[50] J.A. Silveira, C.M. Gamage, J.C. May, D.H. Russell, A periodic-focusing DC-only ion funnel for a cryogenic ion mobility-mass spectrometer, in: 58th ASMS Conference on Mass Spectrometry and Allied Topics, Salt Lake City, UT, 2010.